An Inertial Uni-Axial Interferometer-Based Accelerometer for Harsh Environments

Gerard Aliana Cervera, Santiago Andrés Solis Paiva, Pablo Serrano Gálvez, Jorge Sola Merino, Mark Butcher, Eloise Matheson, and Mario di Castro

***Abstract*—For high-impact devices, subsequent vibrations have as much influence on the deterioration of the mechanical structure as the impact itself. To mitigate the consequences of both impacts and resulting vibrations, it is crucial to accurately understand the peak acceleration and vibration frequencies that originate in the structure. In this article, a radiation tolerant opto-mechanical sensor based on an absolute measurement inertial accelerometer is presented. This method of measurement is chosen due to the viability of placing the readout electronics far from the highly radioactive environment that the sensor may be installed in. The designed accelerometer consists of a fixed aluminum frame with a built-in membrane that acts as a leaf spring. In the same membrane, a retro-reflector is attached which acts as a seismic mass. The retro-reflector reflects the light beam coming from the collimator lens placed on the frame. To prove its viability, the device has been tested under different conditions. First, the device is calibrated and validated using a high-frequency exciter. Second, a high-acceleration testbench is used to compare its output signal with a commercial accelerometer and verify its proper operation as well as its expected lifetime. The experimental results showed an average sensitivity of 9×10^{-4} g/pm with reading measurements of up to 5000 g and a working bandwidth located between 50 and 800 Hz.**

***Index Terms*—Accelerometer, bandwidth, finite element modeling, high impact, inertial sensor, radioactive hazard.**

I. Introduction

INERTIAL sensors have been used for over a century. Depending on the frequency range of interest, three types are commonly used to measure vibrations from an absolute measurement point of view: accelerometers, geophones, and seismometers, whose comparison can be found in [1].

For more than 40 years, seismometers have reached sufficient resolution and dynamic range to capture seismic signals in a broad frequency range [2], [3], [4], [5], including commercial versions [6], [7], [8]. However, there is still a continuous demand for high-end instruments, better adapted to specific applications. In this respect, recent developments in optical technologies offer interesting perspectives for novel inertial sensors capable of operating in harsh environments without nearby electronics or, insensitive to high temperature and pressure. Examples of specific use cases can be found in the nuclear energy field, for example miniature autonomous optical inertial accelerometers have been developed for nuclear tests [9], [10]. Other devices have been reported using optic fibers, such as the fiber interferometer [11], [12], [13], [14], [15], [16], [17], the Fabry–Perot interferometer [18], using fiber Bragg gratings [19], [20], grating sensors [21], multimode interference (MMI) sensors [22], or those based on the ROTE effect [23].

However, to the best of the authors' knowledge, there is no commercial seismometer capable of fulfilling the requirements for applications in high multidirection accelerations at low frequencies, under radiation and magnetic fields, with a fast mounting system and a compact dimension. In this article, a small, passive, novel uni-axial acceleration measurement

Manuscript received 16 August 2022; revised 24 September 2022; accepted 25 September 2022. Date of publication 4 October 2022; date of current version 14 November 2022. This work was supported by the Mechatronics, Robotics and Operations Section (BE-CEM-MRO), European Organization for Nuclear Research (CERN). The associate editor coordinating the review of this article and approving it for publication was Dr. Cheng-Yao Lo. *(Corresponding author: Gerard Aliana Cervera.)*

Gerard Aliana Cervera was with the Mechatronics, Robotics and Operations Section (BE-CEM-MRO), European Organization for Nuclear Research (CERN), Meyrin, 1211 Geneva, Switzerland. He is now with the École Polytechnique Fédérale de Lausanne (EPFL), 1015 Lausanne, Switzerland (e-mail: gerardalianacervera@gmail.com).

Santiago Andrés Solis Paiva, Eloise Matheson, and Mario di Castro are with the Mechatronics, Robotics and Operations Section (BE-CEM-MRO), European Organization for Nuclear Research (CERN), Meyrin, 1211 Geneva, Switzerland (e-mail: santiago.andres.solis.paiva@cern.ch; jeloise.matheson@cern.ch; mario.di.castro@cern.ch).

Jorge Sola Merino was with the Mechatronics, Robotics and Operations Section (BE-CEM-MRO), European Organization for Nuclear Research (CERN), Meyrin, 1211 Geneva, Switzerland. He is now with Advantics, 0450 Saint-Genis-Pouilly, France (e-mail: jorgesome@hotmail.com).

Pablo Serrano Gálvez was with the Mechatronics, Robotics and Operations Section (BE-CEM-MRO), European Organization for Nuclear Research (CERN), Meyrin, 1211 Geneva, Switzerland. He is now with Bobst, 1891 Mex, Switzerland (e-mail: serranogalvez@gmail.com).

Mark Butcher was with the Mechatronics, Robotics and Operations Section (BE-CEM-MRO), European Organization for Nuclear Research (CERN), Meyrin, 1211 Geneva, Switzerland. He is now with Distalmotion, 1066 Epalinges, Switzerland (e-mail: mejbutcher@yahoo.com).

Digital Object Identifier 10.1109/JSEN.2022.3210369

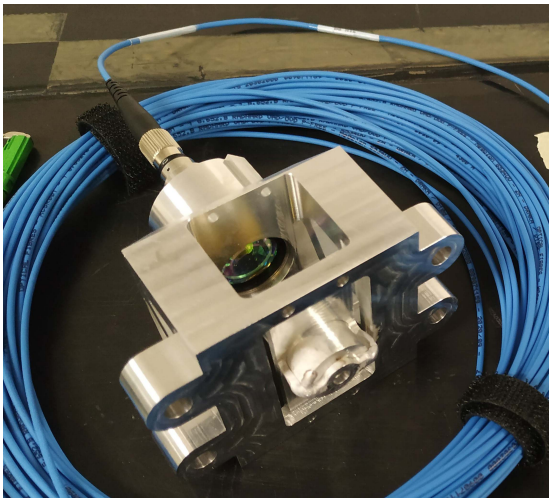

Fig. 1. Final design of inertial uni-axial interferometer-based accelerometer before installation.

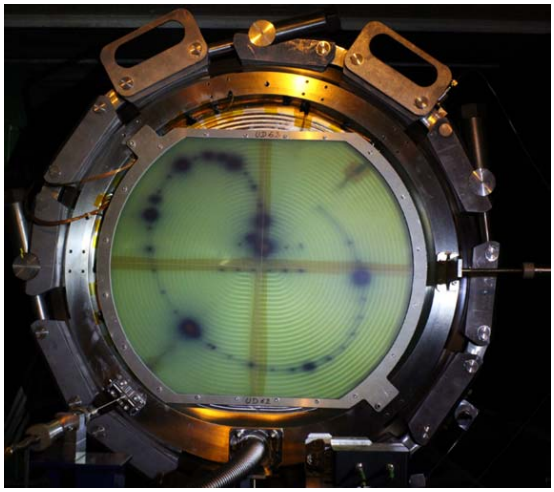

Fig. 2. Gafchromic foil showing the shape of the beam.

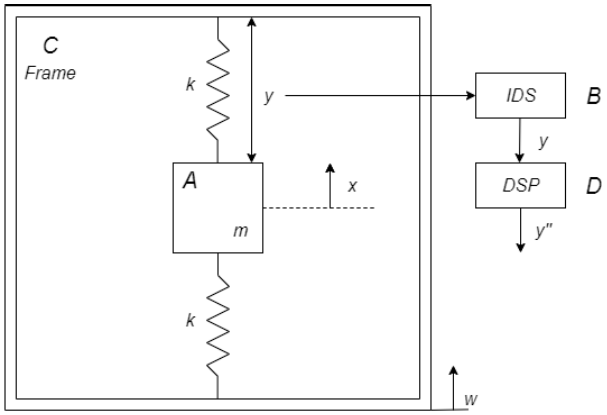

Fig. 3. (A) Schematic of the device with a single degree of freedom (d.o.f.): an oscillating mass, (B) interferometric displacement sensor to measure *y* (C), aluminum structure to hold all the systems together, (D) aquisition processing unit.

sensor is presented. This design is based on the behavior of a piezo-resistive cantilever accelerometer [24] with an improved resistance to signal loss and side accelerations due to the leaf spring system, with the electronics of the sensor placed far from the radioactive source.

This article is organized as follows. The problem formulation and operation principle are presented in Section II. Section III shows the components and manufacturing process of the sensor. Section IV explains the simulations and constrains applied to the 3-D model to ensure its viability during the testing and operation. Section V contains the explanation and results of the experimental validations and Section VI contains results from the first beam test done in 2021. Section VII explains directions for improvements and Section VIII draws the conclusion.

II. Background

During this section, the problem that motivated the research of the sensor that can be seen in Fig. 1, along with the sensor's working principle.

A. Problem Formulation

In high-impact devices designed for long lifetimes, the vibration frequency caused by several impacts has as much influence as the impact amplitude itself on the deterioration of the mechanical structure.

To analyze the consequences of those vibrations and impacts, the acquisition of the peak acceleration and the vibration frequencies that this structure receives is a crucial step. The proposed system has been designed and built specifically to monitor the two improved models of the beam dumps for the large hadron collider (LHC) at the European Organization for Nuclear Research (CERN), Geneva, Switzerland. These dumps, also known as target dump external (TDE), are required to stop and absorb an expected energy of 539 MJ per beam [25] in case of activity or an emergency stop. The monitoring of the dumps will be carried out during LHC Run 3, which begins in 2022.

Due to the collisions occurred, the dumping system and its cavern become highly radioactive. Taking this into account, a passive mechanical sensing system should be used, along with a fiber-optic data transmission system to avoid the failure of the electronic system due to the radiation.

The impact from the beam into the dump device is expected to arrive via a helical shape, creating accelerations on the dump in transversal and vertical directions as shown by Wiesner [26]. This helicoidal shape can be seen in Fig. 2, showing the shape that two weeks of impacts leave on a gafchromic foil placed in front of the dump. Due to these accelerations and the desire of decomposing them on a three-axis Cartesian coordinate system, three uniaxis accelerometers with a low sensitivity to side accelerations are needed. In terms of vibration frequency, the expected vibration generated is around 200 Hz.

Optical-fiber sensors are known to have numerous advantageous features, such as:

1) immunity to electromagnetic interference (EMI) and magnetic fields;
2) rad-hazard resistance;
3) lightweight with low-loss transmission line;
4) potential high sensitivity.

However, only a few optical sensors have made their way from idea and feasibility projects to commercially available products. Some of the usual problems are due to:

1) costly components;
2) need of precise alignment;

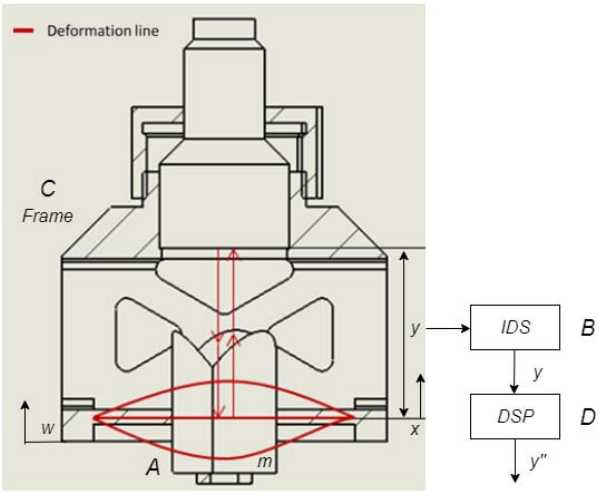

Fig. 4. Section of the proposed device with the components and the expected deformation line.

3) temperature and vibration-induced intensity and phase noise.

B. Operation Principle

As shown in Fig. 3, the accelerometer consists of a seismic mass m, attached to the measurement point by suspension represented by two springs k. The measured movement of the seismic mass is represented by y, the displacement of the element to measure by w.

The movement of the seismic mass is measured by a displacement measuring interferometer (IDS), specifically a mono-axis Fabry–Perot interferometer. As stated by Hecht [27], this type of equipment makes use of the multiple interference phenomena which happens when light enters a cavity bounded by two parallel reflective surfaces. A portion of the light is transmitted out when it comes into contact with one of the surfaces, and the remaining part is reflected back. The end result is that a single beam is split into multiple beams which interfere with each other.

In this project, the interferometer produces a monochromatic laser beam that is guided by an optic fiber into a collimator head. In this head, a small part of the interferometer beam is reflected back on the sensor, producing the reference beam. The remainder of the laser light is focused into the seismic mas [a corner cube retroreflector (CCR)] that acts as a mirror. This remainder is reflected back to the sensor head of the IDS. The reference and the reflected beams interfere with each other producing a distance dependent signal that is detected by the interferometer photodetector. The movement of this CCR will allow us to determine the acceleration after using a precalculated gain as explained in Section V.

Fig. 4 shows a section of the proposed design, include an expected deformation line of the membrane while oscillating. It includes a representation of the IDS and the digital signal processor (DSP). Both systems can be placed far from the sensor structure. The IDS is connected by optic fiber with the collimator head, attached on the sensor as explained in Section III-C.

From the schematics of Fig. 3, the dynamics of the sensor where the equilibrium conditions are represented by

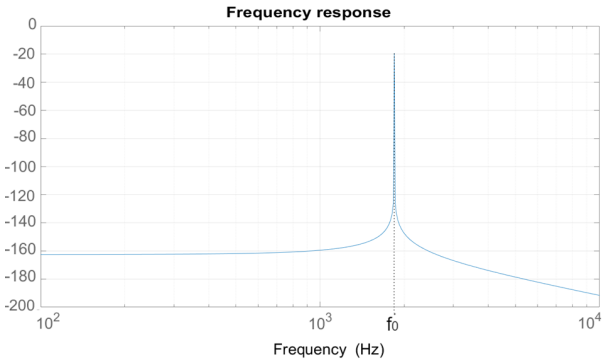

Fig. 5. Transmissibility of the sensor described in Section 3 between $Y(s)$ and $\ddot{W}(s)$.

$x(t) = 0$ reads

$$m\ddot{x}(t) + 2k(x(t) - w(t)) = 0 \tag{1}$$

where $x(t)$ and $w(t)$ are as shown in Fig. 3. The measurement of $y(t) = x(t) - w(t)$ is used to evaluate $w(t)$. After applying, the Laplace transform (1) becomes

$$ms^2Y(s) + 2kY(s) = -ms^2W(s). \tag{2}$$

From (2), the transmissibility $T_{yw}(s)$ between displacement of the moving element $W(s)$ and the relative displacement $Y(s)$ is given by

$$T_{yw}(s) = \frac{Y(s)}{W(s)} = \frac{-ms^2}{ms^2 + 2k}. \tag{3}$$

From (3), we can calculate the relation between the acceleration of the moving element $\ddot{W}(t) = s^2W(s)$ and the relative displacement $Y(s)$, given by

$$T_{y\ddot{w}}(s) = \frac{Y(s)}{s^2W(s)} = \frac{-m}{ms^2 + 2k} = \frac{-1}{s^2 + \frac{2k}{m}}. \tag{4}$$

In order to evaluate k, we need the resonance frequency of the oscillator found in

$$f_0 = \frac{1}{2\pi}\sqrt{\frac{2k}{m}}. \tag{5}$$

The spring constants along the y-axis for each plate spring, which are coupled to the structure to restrain angular rotation, are

$$k = \hat{E}b\left(\frac{h}{l}\right)^3 \tag{6}$$

where $\hat{E} = E/(1 - \upsilon^2)$ due to the ratio b/h bigger than 5 as stated by Storgaard-Larsen et al. [20].

Using the variables from Table I on (5) and (6), a resonance frequency of the main plate of 1843 Hz is reached.

As can be seen in Fig. 5 and due to the flatness of the response of $T_{y\ddot{w}}(s)$ below f_0, the measure of $y(t)$ can be used as an estimator of the acceleration $\ddot{w}(t)$. The absolute value of the frequency response is obtained for $s = jw$.

TABLE I
MATHEMATICAL VARIABLES

Simbology	Variable	Value
m	Seismic mass	0.016 kg
E	Young modulus Aluminium 7075	71.7 GPa
υ	Poisson ratio Aluminium 7075	0.33
b	Width of the membrane	0.02305 m
h	Thickness of the membrane	0.002 m
l	Length of the membrane	0.024 m

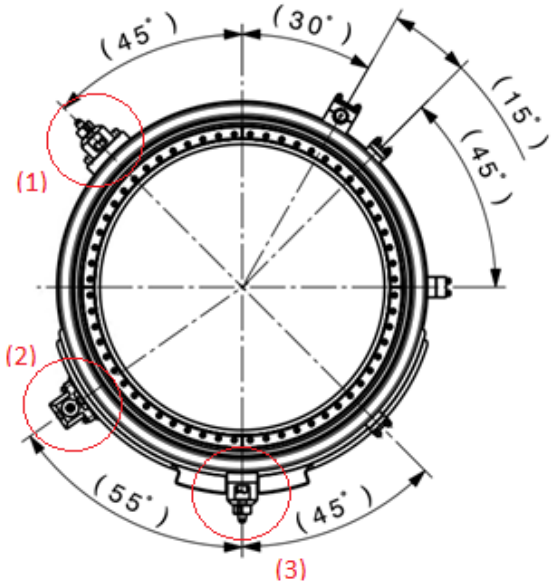

Fig. 6. Distribution of the accelerometers along the LHC dumps diameter as: (1) transversal axis measurement, (2) beam dump axis measurement, and (3) vertical axis measurement.

C. Design Requirements

After several previous tests and calculations from the dump management team shown in [25], the requirements for the inertial-accelerometer were defined as

1) radiation tolerant;
2) readout electronics placed ≈80 m from the source;
3) temperature range between 15 °C and 30 °C;
4) minimum membrane natural frequency of 1500 Hz;
5) maximum beam direction acceleration of 2000 g;
6) maximum transversal to beam direction acceleration of 750 g;
7) maximum vertical to beam direction acceleration of 260 g;
8) minimum life time of 1000 shocks.

A further requirement to achieve a resolution as fine as possible is a minimum displacement of the retro-reflector by 0.1 mm at maximum acceleration.

III. PROPOSED SOLUTION

The sensor consists of four main parts as shown in Fig. 3: an oscillating mass, an interferometric displacement sensor, an aluminum structure, and an acquisition processing unit.

A. Operation Position

These dumps are surrounded by a concrete shielding to isolate as much radiation as possible, leaving a small gap in each diagonal to install all the required sensors. Due to those space restrictions, there are three accelerometers installed along the diameter of the dump, as can be seen in Fig. 6, one to measure the acceleration in each direction.

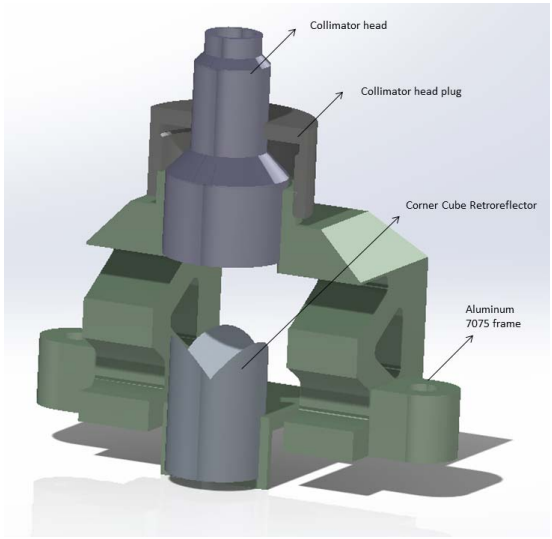

Fig. 7. Components of the inertial accelerometer in operation conditions and its components.

The relationship between the Cartesian axes and the accelerometers distribution is as follows.

1) Indirect measurement of the transversal direction in a 45° angle by decomposing the signal due to the lack of space on the side to install it perpendicularly to 3.
2) Direct measurement of the beam direction at a 55° angle.
3) Direct measurement of the vertical axis from under the dump.

Due to the difficulty of placing the sensor in a suitable position for a direct measurement of the beam direction with the attachment brackets as seen in Fig. 1, an adapted attachment position on the accelerometer was made. This version has the attachment brackets built on the side of the frame, while the membrane behavior matches the original design.

For the optical transfer, an optic fiber connects the sensors with the closest shielded electronics rack, placed 80 m away from the dump.

B. Interferometric Components

The IDS in this system is an IDS3010 [28] from Attocube. This interferometer has three input axes, making it capable of measuring three different distances, with a resolution of 1 pm and a repeatibility of 2 nm. The maximum allowable velocity of the system is 2 m/s with a bandwidth of 10 MHz.

The mounted collimator head [29] has an alignment wavelength of 1550 nm and a focal length of 37.13 mm.

The CCR [30] is made from aluminum with a reflective coating of gold with a quality of 60-40 scratch-dig. The return beam accuracy is of 5 arc second. This piece also allows a 0.2 mm of lateral deflection before losing the signal.

C. Mechanics

On the basis of a typical inertial accelerometer structure, a leaf spring is used as the elastic support in this study. As shown in Fig. 7, the leaf spring is manufactured along with the structural frame from the same block of aluminum, to avoid possible vibration issues on any connection point.

The sensor is 60 mm wide (90 mm including the attachment system), 60 mm long, and 95 mm high, without taking in consideration the needed radius to avoid breaking the optic fiber at the top.

In this device, the CCR also acts as a seismic mass. This seismic mass is placed on the membrane using the built-in brackets to aligned the center of masses of the CCR with the membrane one. This alignment helps to reduce the torque produced on the membrane. The CCR is spot welded on the corners to increase the repeatibility of the system and to avoid possible loosening produced by the vibrations. The spot welding is complemented by an interference of 0.2 mm between the membrane and the upper part of the retroreflector.

The structure is made out of Aluminum 7075 and manufactured using computer numerical control (CNC). Using a unique piece ensures a correct alignment (H7) between the CCR and the collimator head. The structure is designed to hold the collimator head, with negligible deformation compared to the membrane deformation. This unwanted deformation was measured from 0.001 mm (order of magnitude of 2) to a maximum of 0.04 mm (order of magnitude of 1) and never exceeding the 0.2 mm of lateral displacement.

This collimator head is attached with a 0.2-mm diameter by 15 mm length interference. The interference surface includes an external thread and a plug of M30. The plug uses a set screw of M3 to ensure the tightness during the whole lifetime of the system as can be seen in Fig. 7.

The collimator uses an optic fiber connector-type FC/PC, which includes an inner spring to ensure the contact between both fibers. This spring has to be constrained due to a difference between the offsets before and after the impact. The solution found was to use a rad-hazard resistant glue, which also avoids any disconnection due to vibrations.

To reduce the operation time needed to install the accelerometer to less than 10 min due to the environment of the dumps, the system uses 4 × M6 screws with Nordlock blocking washers to ensure the tightness over time. This screws go into a prewelded steel piece with a hole in the middle to allow the membrane to move freely.

D. Acquisition and Processing

The data acquisition system (DAQ) that is used during the operation of this sensor consists of a 18 bits DAQ board by National Instrument, PXIe-1078, and a signal conditioning board. The sampling frequency is set at 40 kHz. This same setup is used for testing.

A low-pass filter of 1000 Hz is applied on the acquired data to remove the resonance frequencies and the noise from the signal data. However, this filter introduces a delay on the data. Another applied filter is a high-pass filter with a 5-Hz cutoff frequency that compensates the initial discordance of the offset due to physical movement of the connection fiber mentioned in Section III-C.

IV. Simulation

The accelerometer, as defined in Section II-C, must meet the technical requirements needed to ensure its viability. To ensure the requirements of the system during its expected operational lifetime, the CAD model has been computer simulated using ANSYS 19.1. The studied simulations are: deformation simulation, stress simulation, reaction force, model analysis, and frequency response (deformation and velocity).

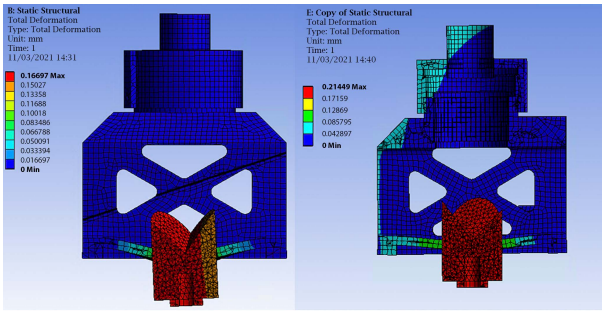

Fig. 8. Operation simulation of the deformation of the system.

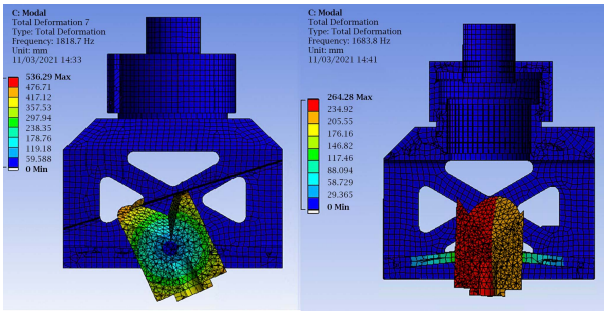

Fig. 9. Modal analysis simulation of the deformation of the system.

TABLE II
Operation Simulation Results

Attachment type	Resonance frequencies	Statics deformation	Maximum velocity	Reaction force
Vertical	1818.7 Hz	$1.66{\cdot}10^{-4}$ m	$1.7{\cdot}10^{-3}$ m/s	2485 N
Lateral	1778 Hz	$2.1{\cdot}10^{-4}$ m	$2.67{\cdot}10^{-3}$ m/s	6695 N

A. Operation Simulation

The conditions applied to this simulation are as follows.

1) The acceleration expected on the three different directions is applied to the whole system.
2) The fixation system is simulated using the holes for the attachment as fixed points.

The results from the deformation analysis and modal analysis are shown graphically in Figs. 8 and 9 and the numerical results in Table II.

B. Calibration Simulation

Due to misalignment between the shaker used for calibration (see Section V-A) and the attachment of the accelerometer, an adapter piece was designed to interface between the shaker and accelerometer. To ensure the correct calibration of the system, the first resonance frequency must be the one generated by the motion of the membrane.

The conditions applied to this simulation are as follows.

1) The acceleration delivered by the shaker is applied to the whole system. Due to the weight of the sensor, the acceleration is limited to 7 g.
2) The fixation system between the adapter piece and the sensor is simulated using the fixing points between the models.
3) The fixation system to the shaker is simulated using the holes for the attachment of the adapting piece.

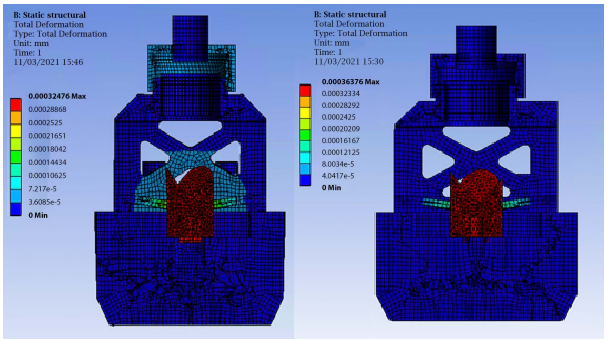

Fig. 10. Simulation of the deformation of the system during the calibration.

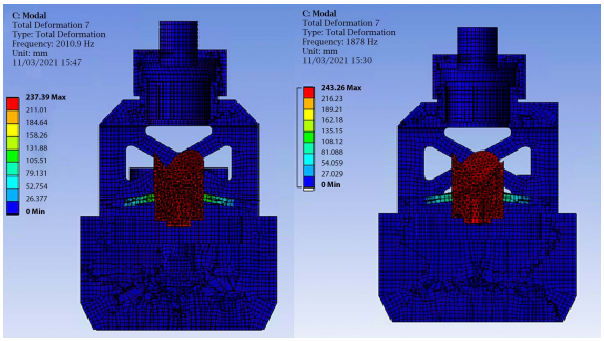

Fig. 11. Modal analysis of the system during the calibration.

TABLE III
CALIBRATION SIMULATION RESULTS

Attachment type	Resonance frequencies	Statics deformation	Maximum velocity	Reaction force
Vertical	2010.9 Hz	$3.3{\cdot}10^{-7}$ m	$1.5{\cdot}10^{-3}$ m/s	46.5 N
Lateral	1878 Hz	$3.3 \cdot 10^{-7}$ m	$3.9{\cdot}10^{-3}$ m/s	44.6 N

The results from the deformation analysis and modal analysis can be shown graphically in Figs. 10 and 11 and the numerical results can be observed on Table III.

V. EXPERIMENTS

This section describes the experiments carried out on the presented sensor to characterize and test it.

A vibration exciter was used for the gain calibration along with the dynamic behavior confirmation tests and a high acceleration test-bench for impact response and lifetime characterization.

All laboratory tests were made at room temperature without thermal stabilization as it happens in the dump caverns. The effects of thermal instability should not have had an important role in this project. It is important to observe the effects of unstable temperatures, as may happen under other applications.

A. Vibration Exciter

The vibration exciter was a B&k 4808 [31] capable of exciting its base up to 10 000 Hz with a maximum acceleration related to the load. In this case, the maximum achievable acceleration was 7 g applied on the base of the adapter piece. This device had a resonance frequency at 75 Hz due to an EMI that creates a relative peak on the first frequencies. During this phase of the test, it was used to calibrate and test the bandwidth of the sensor.

The adapting piece explained in Section IV-B included a mounted commercial reference accelerometer [32] on the same axis as the center of the CCR. This reference accelerometer was the PCB 352A74, a miniaturized and lightweight sensor capable of reaching 50 g and 8000 Hz with a weight of 1.2×10^{-3} kg. The full assembly of both parts can be seen in Fig 12.

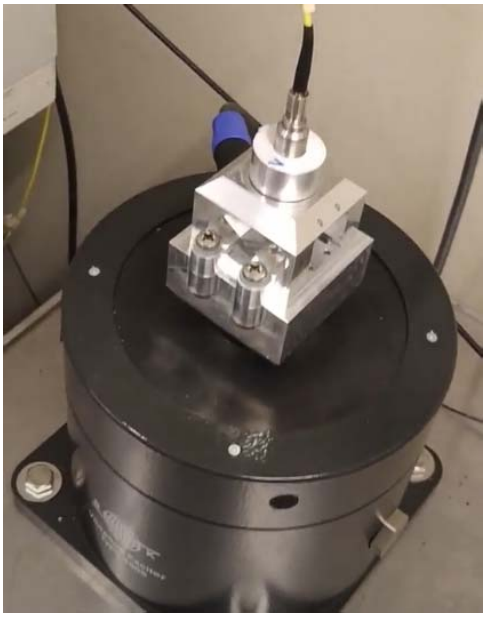

Fig. 12. Picture of the vibration exciter assembly, including the interface piece.

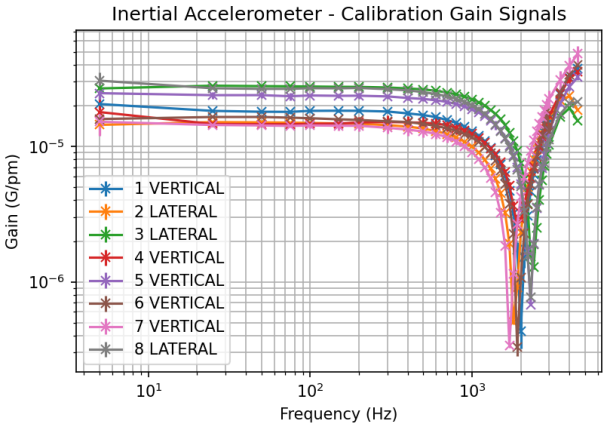

Fig. 13. Calibration gains from all the installed sensors.

1) Calibration: A frequency sweep was performed to characterize the bode diagram and extract the calibration gain in the passband region.

The excitement applied on the accelerometer was 7 g when it was far from the resonance frequency and 5 g when it was getting close to it, to avoid reaching the mechanical limits of the vibration exciter. This sweep was applied on the 5–4500 Hz range, in steps of 100 Hz.

As it can be seen in Fig. 13, the resonance frequencies were found between 1700 and 2400 Hz. This difference was due to the misalignment in the centering of the CCR and the tolerances produced on the H7 hole mentioned in Section III-C, which leads to lower interference.

In these plots, an increased deviation at the first point can be observed. That was due to the low gain that occurred because of the low frequency and the resonance frequency of the vibration exciter mentioned before, which affected the repetition of the test.

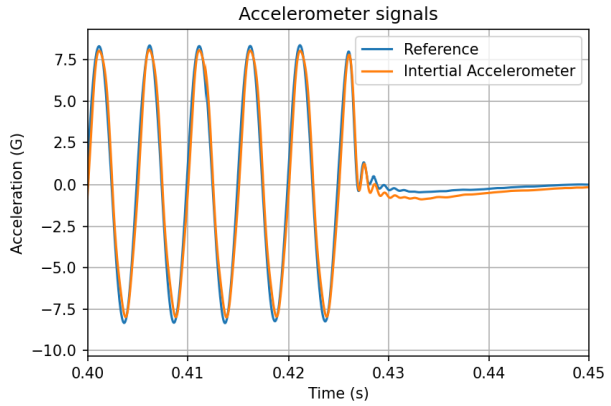

Fig. 14. Vibration exciter result from the zero signal introduced test.

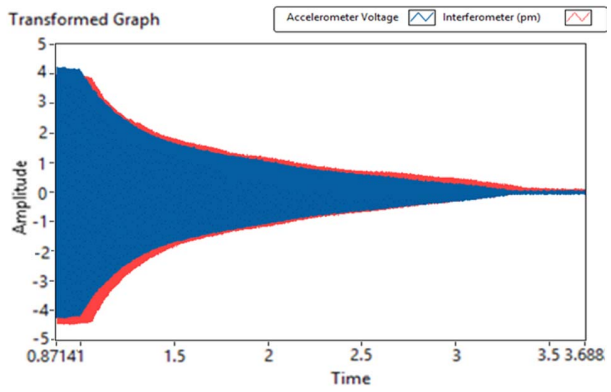

Fig. 15. Vibration exciter result from the damping test.

2) Zero Signal Introduced: Another repeatability test performed was to introduce a zero signal into the accelerometer to force an abrupt stop. First, the vibration was stabilized using 7 g and 200 Hz, knowing that it was going to be the operation frequency. After the signal was purely sinusoidal, the zero acceleration was introduced. Both accelerometer signals are compared. This test was performed several times to check the repeatability of the signal.

As it can be seen in Fig. 14, both signals match well. It can be observed how the optical sensor keeps oscillating due to the inertia, but this damping follows the signal of the reference accelerometer. The difference between both signals at the highest acceleration is 0.5 g.

3) Damping Test: The last performed test using the vibration exciter was to observe a slower damping of the acceleration. To check this situation, the signal was stabilized with the same specifications as with the previous test. After this, the acceleration was slowly decreased until 0 g.

As it can be seen in Fig. 15, the given signals are similar, including the small delay produced by the high-pass filter at 5 Hz.

B. High Acceleration Test Bench

The device was tested in a high acceleration testbench with a similar impact as the one expected for its final application. For this purpose, an impact test-bench capable of reaching 8000 g and 10 000 Hz was designed and built [33].

The proposed device was composed of two subsystems, the impact and the automation subsystems, as it can be seen in Fig. 16.

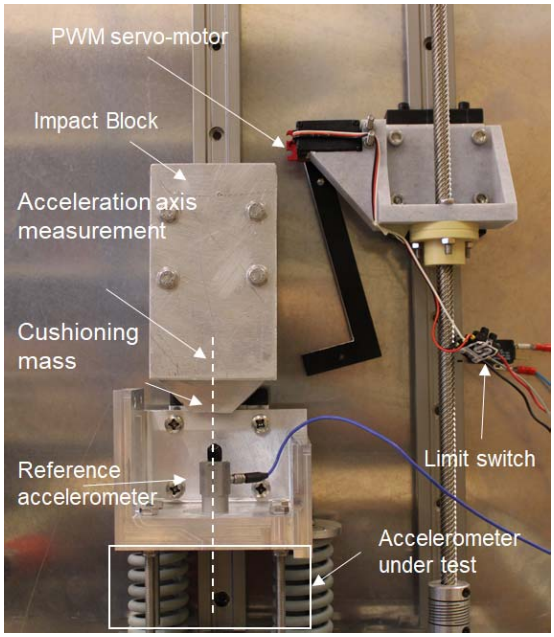

Fig. 16. Impact test bench and components.

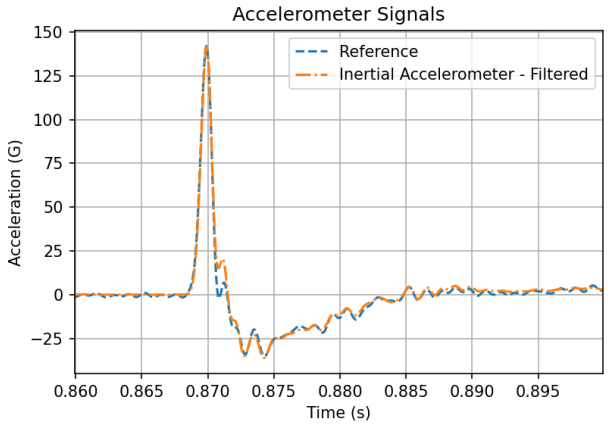

Fig. 17. Impact data from the reference and the in-house accelerometers.

The impact subsystem consisted of an assembly holding both the accelerometer-under-test and a reference accelerometer on the same axis. It had high stiffness and was attached to a linear bearing. It rested on a spring-loaded damping block assembly that compressed at the moment of the impact of a dropping mass (metal-metal contact to increase the energy transmission) from a height of up to 0.57 m, depending on the acceleration needed. The output signals of the accelerometer-under-test and the reference accelerometer were acquired synchronously for comparison. This reference accelerometer was the PCB 301A12 [34], capable of reaching 10 000 g and 10 000 Hz under normal circumstances, with a weight of 4.2×10^{-3} kg.

The automation subsystem raised the impact mass up to the selected position and dropped it. This process was repeated for a preselected number of cycles. The mechanism used a lead screw attached to a stepper motor that lifted a guided platform. A servomotor was attached to the platform with the purpose of engaging and disengaging the mass. The impact mass is also attached to the linear bearing of the accelerometer.

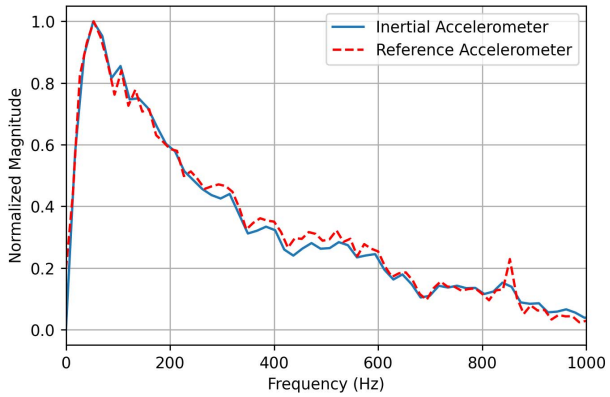

Fig. 18. Vibration exciter result from the zero signal introduced test.

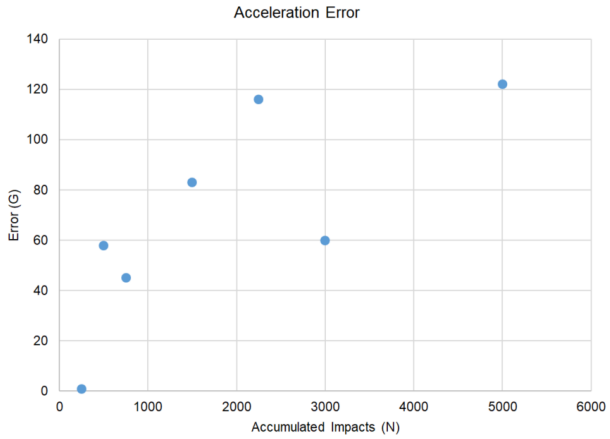

Fig. 19. Measurement error from the lifetime data.

1) Impact Test: The first parameter to verify with this test-bench was the correct response between the reference accelerometer and the proposed sensor in this article. To check this response, an impact acceleration of 150 g and a frequency of 200 Hz are used. Due to the number of impacts required to verify the response of the sensor at this frequency, 150 g was the maximum acceleration that could be applied with an acceptable repeatable error of ± 30 g.

As it can be seen in Fig. 17, the accelerometer gives the same response to the main impact, with some disturbances during the dumping. The only misalignment produced was after the first impact, where the proposed accelerometer had a second impact 0.001 s before the reference one. Regarding the achieved frequencies, as it can be seen in Fig. 18, the frequency magnitudes of both accelerometers are similar, with an undetected peak by the in-house accelerometer at 850 Hz.

2) Life Time Test: Another important parameter to characterize was the model's impact cycles resistance and how these impacts affected the accuracy during time.

For this purpose, the automation feature was used, reaching 2000 g at a non-controlled frequency. This test was done as long as the hardware components of the system withstands, regardless of the precision of the acquired data. An acquisition every 250 cycles at 200 g and 200 Hz was taken.

As it can be seen in Fig. 19, the reliability of this system started losing accuracy from 750 cycles, where the rad-hazardous glue begun its deterioration. This damage implied that the subsequent accelerations after the beam impact are not read correctly, but the main one is still valid.

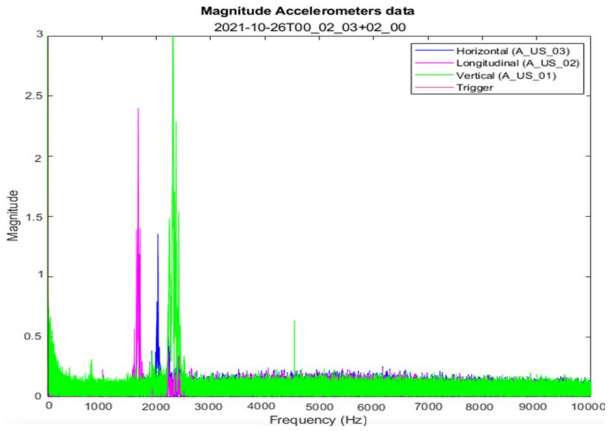

Fig. 20. Operational test showing the raw data of the accelerometers.

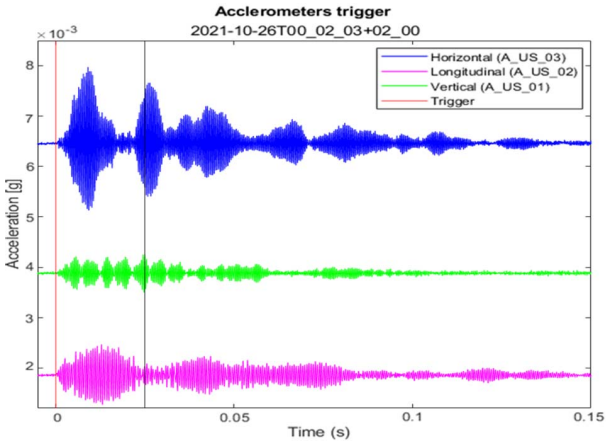

Fig. 21. Operational test after post-processing.

From 1500 impacts, the rubber fixing the connector to the fiber breaks down. It loses the signal frequently, and the readouts are inconsistent, leaving this number of cycles as the failure point.

This same configuration is used to confirm the simulations where the moving speed of the retroreflector does not surpass the 2 m/s limit, which would imply a loss of signal from the IDS. This confirmation was produced when the DAQ did not detect any signal discontinuity when the impact happened.

VI. Operational Results

On October 26, 2021, the first beams for the new long run of the LHC were dumped on the TDE. The reading of this dump, that received an energy from the beam of 1.8×10^{11} ppb, can be seen in Figs. 20 and 21.

As shown in Fig. 20, all three accelerometers reach its resonance frequencies at around 2000 Hz, where the magnitude of their readings becomes inconsistent with reality. Some magnitude peaks can also be seen under 500 Hz, the reading bandwidth of the sensor.

After the post-processing of the data, the readings of the sensor acquire physical meaning as accelerations, as seen in Fig. 21. It can be observed how all three sensors noticed the beam dump as stated by the trigger line, with a bigger impact on the horizontal direction, depending on the moment of impact inside the helicoidal shape shown in Fig. 2.

VII. Discussion

Because of the substantial seismic mass (0.016 kg), the relatively high compliance of the spring elements (Aluminum

7075 membrane) in the accelerometer and the range (between 15 °C and 30 °C, where this system is planned to work), the thermal mechanical noise is not expected to have significant influence on the detection range of this device.

When compared to most of the commercial inertial sensors, this device does not use coil inside the sensing elements, resulting in an amplification of the response at the sensors resonance and making it compatible with magnetic fields. Comparing this sensor with the state of the art, it offers several important advantages: 1) compact form of uni-axial measurement of the sensing elements; 2) mechanical alignment between the head and the retroreflector, reducing the probability of misalignment; 3) low sensitivity from side collisions due to the used components and structure; 4) high resistance to impacts up to 8000 g; and 5) easy installation procedure, allowing it to be done in short time.

The main limitation of this accelerometer is the resonance frequency, which was 1700 Hz in the worst case scenario, combined with the maximum velocity of 2 m/s, allowed by the interferometric readout electronics. Those two factors are proportional, which means that with this shape and material it becomes difficult to increase the frequency range. Another limitation comes with the cycles this device receives, where the radiation resistant glue applied on the optic fiber connection degrades, making it unreliable from 1500 impacts.

Furthermore, the sensitivity of the accelerometer can be improved by increasing the seismic mass of the CCR or by decreasing the thickness of the membrane. Both methodologies reduce the resonance frequency and, as consequence, decrease the upper limit on frequency by increasing its precision.

The bandwidth can be increased by improving the lateral stiffness of the membrane, so the torque produced by the lateral impacts does not result in the first natural frequency of the system. This increase leads to the membrane natural frequency of 3700 Hz according to the simulations.

VIII. Conclusion

In this article, the modeling and calculations that describe the properties of a novel opto-mechanical sensor based on the use of interferometry, and experimental results concerning the characterization and testing of such a device, have been presented. It has been shown that a uni-axial optical accelerometer capable of minimizing the side accelerations produced on the system can be fabricated. Despite all the design constraints, a sufficiently high bandwidth is reached, which can be further improved if other materials and readout electronics are used.

As an average scenario, the in-plane acceleration with a minimum bandwidth of 800 Hz (−3 dB variation) can be detected by the optical accelerometer with a sensitivity of 9×10^{-4} g/pm and a range up to 5000 g, without losing the signal. The consistency of those readouts can be ensured up to 750 impacts of 2000 g. The accelerometer can be applied in high acceleration systems, rad-hazardous environment, and other similar applications.

Acknowledgment

The authors thank the technicians team from the European Organization for Nuclear Research (CERN), Geneva, Switzerland, which helped manufacturing the prototypes. They also thank Annabella Zamora from CERN for useful discussions and her comments on the manuscript.

References

[1] C. Collette et al., "Review: Inertial sensors for low-frequency seismic vibration measurement," *Bull. Seismolog. Soc. Amer.*, vol. 102, no. 4, pp. 1289–1300, Aug. 2012.
[2] H. E. Sheffield, "An electronic vertical long-period seismometer," *IEEE Trans. Instrum. Meas.*, vol. IM-13, no. 1, pp. 2–7, Mar. 1964.
[3] C. Teupser and A. Plešinger, "Design of feedback-controlled wide-band seismographs with respect to undesired side-effects," *Phys. Earth Planet. Interiors*, vol. 18, no. 2, pp. 58–63, Feb. 1979.
[4] M. J. Usher, R. F. Burch, and C. Guralp, "Wide-bandfeedback seismometers," *Phys. Earth Planet. Interface*, vol. 18, pp. 38–50, Feb. 1979.
[5] E. Wielandt and G. Sterkeisen, "The leaf spring seismometer: Design and performance," *Bull. Seismolog. Soc. Amer.*, vol. 72, pp. 2349–2367, Dec. 1982.
[6] *Fiber Optical Accelerometer*, Sercalo Microtechnology Ltd, Neuchatel, Switzerland.
[7] *MR660 Multi-Axis Fiber Optic Accelerometer*, Micronor LLC, Camarillo, CA, USA.
[8] *FS65 Optical Accelerometer for Low Frequencies*, HBM, Paris, France.
[9] D. Carr, G. Bogart, S. Goodman, P. Baldwin, and D. Robinson, "A laser interferometric miniature seismometer," in *Monitoring Research Review: Ground-Based Nuclear Explosion Monitoring Technologies*. Portsmouth, NH, USA, 2008.
[10] D. Carr, P. Baldwin, S. Knapp-Kleinsorge, H. Milburn, and D. Robinson, "A laser interferometric miniature seismometer," in *Monitoring Research Review: Ground-Based Nuclear Explosion Monitoring Technologies*. Portsmouth, NH, USA, 2010, p. 268.
[11] D. Gardner, T. Hofler, S. Baker, R. Yarber, and S. Garrett, "A fiber-optic interferometric seismometer," *J. Lightw. Technol.*, vol. 5, no. 7, pp. 953–960, Jul. 5, 1987.
[12] A. Araya, K. Kawabe, T. Sato, N. Mio, and K. Tsubono, "Highly sensitive wideband seismometer using a laser interferometer," *Rev. Sci. Instrum.*, vol. 64, no. 5, pp. 1337–1341, May 1993.
[13] A. Araya, K. Sekiya, and Y. Shindo, "Broadband seismometer for ocean borehole observations," in *Proc. Symp. Underwater Technol. Workshop Sci. Use Submarine Cables Related Technol.*, 2007, pp. 245–248.
[14] F. Acernese, G. Giordano, R. Romano, R. D. Rosa, and F. Barone, "Tunable mechanical monolithic sensor with interferometric readout for lowfrequency seismic noise measurement," *Nucl. Instrum. Methods Phys. Res.*, vol. A617, nos. 1–3, pp. 457–458, 2010.
[15] C. Collette, F. Nassif, J. Amar, C. Depouhon, and S.-P. Gorza, "Prototype of interferometric absolute motion sensor," *Sens. Actuators A, Phys.*, vol. 224, pp. 72–77, Apr. 2015.
[16] J. Otero, "Development and characterization of an observatory-class, broadband, non-fedback, leaf-spring interferometric seismometer," Ph.D. thesis, Univ. California, San Diego, CA, USA, 2009.
[17] R.-J. Li, Y.-J. Lei, Z.-X. Chang, L.-S. Zhang, and K.-C. Fan, "Development of a high-sensitivity optical accelerometer for low-frequency vibration measurement," *Sensors*, vol. 18, no. 9, p. 2910, Sep. 2018.
[18] T. yoshino, K. Kurosawa, K. Itoh, and T. Ose, "Fiber-optic Fabry–Pérot interferometer and its sensor applications," *IEEE Trans. Microw. Theory Techn.*, vol. MTT-30, no. 10, pp. 1612–1621, Oct. 1982.
[19] Y. Yu, L. Lui, H. Tam, and W. Chung, "Fiber-laser-based wavelength-division multiplexed fiber Bragg grating sensor system," *IEEE Photon. Technol. Lett.*, vol. 13, no. 7, pp. 702–704, Jul. 2001.
[20] T. Storgaard-Larsen, S. Bouwstra, and O. Leistiko, "Opto-mechanical accelerometer based on strain sensing by a Bragg grating in a planar waveguide," *Sens. Actuators A, Phys.*, vol. 52, pp. 25–32, Apr. 1996.
[21] B. Merchant and M. Okandan, "The SNL MEMS seismometer: Design and testing," Sandia Nat. Lab (SNL-NM), Albuquerque, NM, USA, Tech. Rep. SAND2009-4203C, 2009, p. 352.
[22] K. Wang et al., "Advances in optical fiber sensors based on multi-mode interference (MMI): A review," *IEEE Sensors J.* vol. 21, no. 1, pp. 132–142, Jan. 2021.
[23] A. Jian et al., "Theoretical analysis of an optical accelerometer based on resonant optical tunneling effect," *Sensors*, vol. 17, no. 2, p. 389, 2017.
[24] A. M. Casas-Ramos, L. G. Castillo-Barrera, and G. E. Sandoval-Romero, "Optical accelerometer for seismic measurement," *Vibroeng. Proc.*, vol. 21, pp. 38–41, Dec. 2018.
[25] J. Maestre et al., "Design and behaviour of the large hadron collider external beam dumps capable of receiving 539 MJ/dump," *J. Instrum.*, vol. 16, no. 11, Nov. 2021, Art. no. P11019.

[26] C. Wiesner, "LHC beam dump performance in view of the high luminosity upgrade," in *Proc. IPAC*. Copenhagen, Denmark, May 2017, pp. 1–4.
[27] E. Hecht, *Optics*. Cambridge, MA, USA: Fabry–Pérot Theory, 2015.
[28] *IDS3010 Minitaturized Displacement Measurement*, Attocube Wittenstein Group, Berlin, Germany.
[29] *1550 nm Air-Spaced Doublet Collimator Packages*, document F810FC-1310, Thorlabs Inc, Zürich, Switzerland.
[30] *Hollow Metal Retroreflector, Replicated, 19.1 mm OD, 5 Arc Sec RBA*, Newport Corporation, Paris, France.
[31] *Permanent Magnetic Vibration Exciter Type 4808*, Brüel and Kjær, Copenhagen, Denmark.
[32] *352A74–ICP ACCELEROMETER*, PCB Piezotronics an MTS Company, Depew, NY, USA.
[33] G. A. Cervera, J. S. Merino, M. D. Castro, M. Butcher, and P. S. Galvez, "Automatic validation device for single-axis high impact accelerometers," in *Precision Motion Systems and Control*. Cranfield, U.K.: EUSPEN, 2020.
[34] *301A12—ICP ACCELEROMETER*, PCB Piezotronics an MTS Company, Depew, NY, USA.

Gerard Aliana Cervera received the M.Sc. degree in industrial engineering from the Polytechnic University of Catalunya, Barcelona, Spain, in 2020. He is currently pursuing the M.Sc. degree in materials and manufacturing with Jönköping University, Jönköping, Sweden.

From 2019 to 2021, he was with the Mechatronics, Robotics and Operations Section, European Organization for Nuclear Research (CERN), Geneva, Switzerland. He currently develops his professional career at the École Polytechnique Fédérale de Lausanne (EPFL), Lausanne, Switzerland, in the electron microscopy field. His research interests include sensing elements, design under harsh environments, high precision, and high vacuum.

Santiago Andrés Solis Paiva received the M.Sc. degree in robotics and automation from the Polytechnic University of Madrid, Madrid, Spain, in 2018.

In 2018, he has joined the Mechatronics, Robotics and Operations Section, European Organization for Nuclear Research (CERN), Geneva, Switzerland. His current research interests include machine learning applied to automated systems and high-precision positioning control.

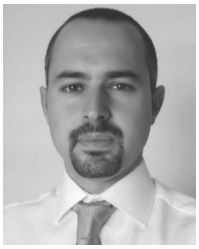

Pablo Serrano Gálvez received the M.Sc. degree in physics from the University of Murcia, Murcia, Spain, in 2009, and the M.Sc. degree in electromechanical engineering (mechatronics) and the Ph.D. degree in electric and electronic engineering from the Polytechnic University of Madrid, Madrid, Spain, in 2013 and 2020, respectively.

From 2014 to 2020, he has worked as a Mechatronic Engineer with the Department of Engineering, Mechatronic, Robotics and Operations Section, European Organization for Nuclear Research (CERN), Geneva, Switzerland. He develops his professional career in the private industry focused on project management, product development, and quality assurance.

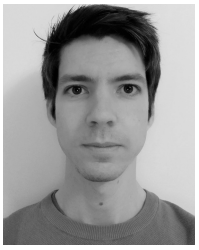

Jorge Sola Merino received the M.S. degree in industrial engineering with specialization in mechatronics from the Universidad Politecnica de Valencia, Valencia, Spain, and the Lunds Tekniska Hogskola, Lund, Sweden, in 2015.

From 2016 to 2020, he has worked with the Mechatronics, Robotics and Operations Section, European Organization for Nuclear Research (CERN), Geneva, Switzerland. His research interests are in the development of control algorithms and electronics for high-precision systems. He develops his professional career in the private industry.

Mark Butcher received the M.Eng. degree in engineering science from the University of Oxford, Oxford, U.K., in 2003, and the Ph.D. degree in automatic control from the Ecole Polytechnique Fédérale de Lausanne, Lausanne, Switzerland, in 2009.

From 2010 to 2020, he has worked with the Department of Engineering, European Organization for Nuclear Research (CERN), Geneva, Switzerland. He develops his professional career in the private industry.

Eloise Matheson received the M.Sc. degree in advanced robotics from the École Centrale de Nantes, Nantes, France, in 2014, and the Ph.D. degree in surgical robotics from the Imperial College London, London, U.K., in 2020.

From 2014 to 2016, she has worked with the Robotics Group, ESA, on teleoperation of space systems. Since 2020, she has been with the Mechatronics, Robotics, and Operation Section, European Organization for Nuclear Research (CERN), Geneva, Switzerland. Her research interests include teleoperation and mechatronics instrumentation.

Mario di Castro received the M.Sc. degree in electronic engineering from the University of Naples "Federico II," Naples, Italy, in 2006, and the Ph.D. degree in robotics and industrial controls from the Polytechnic University of Madrid, Madrid, Spain, in 2019.

From 2007 to 2011, he has worked with DESY in charge of advanced mechatronics for synchrotron beamlines controls. Since 2011, he has been working with the European Organization for Nuclear Research (CERN), Geneva, Switzerland, where he leads the Mechatronics, Robotics and Operation Section, since 2018, responsible for the design, installation, and operation of control systems for movable devices. His research interests include automatic controls and mechatronics.